JACS
JOURNAL OF THE AMERICAN CHEMICAL SOCIETY
pubs.acs.org/JACS
Article

Experimental and Computational Studies on the Ruthenium-Catalyzed Dehydrative C−H Coupling of Phenols with Aldehydes for the Synthesis of 2-Alkylphenol, Benzofuran, and Xanthene Derivatives

Nuwan Pannilawithana, Bimal Pudasaini, Mu-Hyun Baik,* and Chae S. Yi*

Cite This: J. Am. Chem. Soc. 2021, 143, 13428−13440
Read Online

ABSTRACT: The cationic Ru−H complex $[(C_6H_6)(PCy_3)(CO)\text{-}RuH]^+BF_4^-$ (**1**) was found to be an effective catalyst for the dehydrative C−H coupling reaction of phenols and aldehydes to form 2-alkylphenol products. The coupling reaction of phenols with branched aldehydes selectively formed 1,1-disubstituted benzofurans, while the coupling reaction with salicylaldehydes yielded xanthene derivatives. A normal deuterium isotope effect was observed from the coupling reaction of 3-methoxyphenol with benzaldehyde and 2-propanol/2-propanol-d_8 (k_H/k_D = 2.3 ± 0.3). The carbon isotope effect was observed on the benzylic carbon of the alkylation product from the coupling reaction of 3-methoxyphenol with 4-methoxybenzaldehyde (C(3) 1.021(3)) and on both benzylic and *ortho*-arene carbons from the coupling reaction with 4-trifluorobenzaldehdye (C(2) 1.017(3), C(3) 1.011(2)). The Hammett plot from the coupling reaction of 3-methoxyphenol with *para*-substituted benzaldehydes *p*-X-C_6H_4CHO (X = OMe, Me, H, F, Cl, CF_3) displayed a V-shaped linear slope. Catalytically relevant Ru−H complexes were observed by NMR from a stoichiometric reaction mixture of **1**, 3-methoxyphenol, benzaldehyde, and 2-propanol in CD_2Cl_2. The DFT calculations provided a detailed catalysis mechanism featuring an electrophilic aromatic substitution of the aldehyde followed by the hydrogenolysis of the hydroxy group. The calculations also revealed a mechanistic rationale for the strong electronic effect of the benzaldehdye substrates *p*-X-C_6H_4CHO (X = OMe, CF_3) in controlling the turnover-limiting step. The catalytic C−H coupling method provides an efficient synthetic protocol for 2-alkylphenols, 1,1-disubstituted benzofurans, and xanthene derivatives without employing any reactive reagents or forming wasteful byproducts.

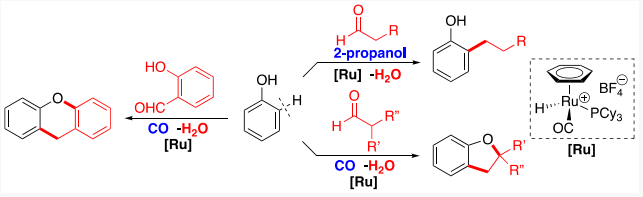

INTRODUCTION

Transition-metal-catalyzed C−H alkylation methods have emerged as some of the most versatile C−C bond formation protocols, which have far-reaching potentials ranging from re-forming biomass feedstocks to the synthesis of complex organic molecules.[1] In comparison to classical Friedel−Crafts type electrophilic alkylation methods, which form a mixture of linear and branched products as well as copious amounts of salt byproducts, transition-metal-catalyzed C−H alkylation methods offer highly chemoselective protocols for forming the desired alkylation products, with an unparalleled opportunity for the late-stage functionalization of organic molecules.[2] Major research efforts have been focused on the development of catalytic C−H alkylation methods that employ readily available alkylating reagents without the formation of any wasteful byproducts.

Since Murai's seminal report on chelate-assisted C−H alkylation of aryl-substituted ketones,[3] a variety of oxygen and nitrogen directing groups have been successfully utilized for promoting regioselective alkylation reactions of arenes.[4] While most of these chelate-assisted C−H insertion methods favor the *ortho*-selective alkylation of arene substrates, a number of *meta*-selective arene C−H alkylation methods have recently been devised by using elaborated directing groups.[5] Such strategies have also found considerable success in advancing regioselective C−H alkylation reactions of non-aromatic olefinic substrates.[6] Chelate assistance protocols have been shown to be particularly effective for devising catalytic sp^3 C−H alkylation methods,[7] and remarkably enantioselective sp^3 C−H alkylation and arylation methods have been achieved by using chiral metal catalysts.[8]

A variety of catalytic sp^3 C−H alkylation strategies have been successfully developed in the last few decades. Cross-dehydrogenative-coupling methods have been shown to be effective for directly forming C−C bonds between two

Received: July 2, 2021
Published: August 16, 2021

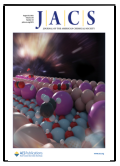

saturated aliphatic substrates.[9] Metal to ligand cooperative bifunctional catalysis protocols have been shown to be effective tools for promoting direct sp^3 C−H alkylation reactions for aliphatic groups adjacent to nitrogen and carbonyl groups.[10] Chen and co-workers devised Pd-catalyzed sp^3 C−H alkylation protocols as an effcient strategy to derivatize α-amino acid substrates.[11] Recently, a number of remarkably chemoselective sp^3 C−H alkylation methods have been achieved by employing photocatalysis strategies, and the most notable examples include the direct β-arylation of cyclic ketones with electron-deficient arylnitriles,[12] remote C(sp^3)−H bond alkylation via proton-coupled hydrogen atom transfer catalysis,[13] and decarboxylative alkylation mediated by triphenylphosphine.[14]

From an economic and sustainability perspective, oxygenated substrates such as alcohols and carbonyl compounds have long been desired reagents for the C−C bond forming reactions because these substrates are readily available from biomass feedstocks.[15] As part of our ongoing efforts to design sustainable catalytic coupling methods, we have been exploring the dehydrative C−H coupling reactions of arenes with a variety of oxygenated hydrocarbon substrates that would form water as the sole byproduct. We previously discovered that the well-defined cationic ruthenium hydride complex $[(C_6H_6)(PCy_3)(CO)RuH]^+BF_4^-$ (**1**) is a highly effective catalyst precursor for a number of dehydrative C−H coupling reactions of arenes with alcohols and carbonyl compounds.[16] We also found that the Ru−H catalyst **1** promotes a highly stereoselective dehydrative C−H coupling reaction of phenols with ketones to form trisubstituted (*Z*)-olefin products.[17] Encouraged by these observations, we sought to extend the synthetic utility of the dehydrative C−H coupling reactions of arenes with various carbonyl compounds. This report delineates a Ru-catalyzed dehydrative C−H coupling method of phenols with aldehydes, which efficiently installs a number of biologically important core structures, such as 2-alkylphenols, benzofurans, and xanthene derivatives. The report also presents comprehensive experimental and computational studies that offer a detailed mechanism featuring an electrophilic aromatic substitution of the aldehyde substrate and the subsequent hydrogenolysis steps in forming the desired alkylation products.

RESULTS AND DISCUSSION

Reaction Discovery and Optimization Study. While exploring the scope of dehydrative C−H coupling of phenols with carbonyl compounds, we initially observed that the reaction between 3-methoxyphenol and 1-hexanal led to the formation of *ortho*-alkylation product **2a** along with a number of side products (eq 1). Recognizing that the formation of the

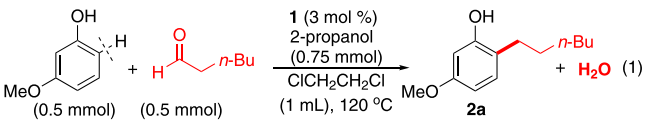

dehydrative coupling product **2a** would require 1 equiv of hydrogen donors, we screened several common hydrogen additives. The addition of H_2 (5 atm) or 2-propanol (1.5 equiv) significantly improved the yield and selectivity for the alkylation product **2a** (Table 1, entries 1 and 2). Both the cationic Ru−H complex **1** and the *in situ* generated catalyst from the reaction of the tetranuclear Ru−H complex with $HBF_4{\cdot}OEt_2$ exhibited the highest activity and selectivity for

Table 1. Catalyst Screening and Optimization for the Dehydrative Coupling of 3-Methoxyphenol with 1-Hexanal[a]

entry	catalyst	deviation from the standard conditions	**2a** (%)[b]
1	**1**	none	72
2	**1**	H_2 (5 atm)	72
3	**1**	no 2-propanol	37
4	**1**	1,4-dioxane	25
5	**1**	chlorobenzene	16
6	**1**	toluene	25
7	**1**	2-propanol (1 mL)	32
8	$[(PCy_3)(CO)RuH]_4(O)(OH)_2/HBF_4{\cdot}OEt_2$		70
9	$(PCy_3)_2(CO)RuHCl/HBF_4{\cdot}OEt_2$		29
10	$RuCl_2(PPh_3)_3/HBF_4{\cdot}OEt_2$		23
11	$RuCl_3{\cdot}3H_2O$		0
12	$Ru_3(CO)_{12}/HBF_4{\cdot}OEt_2$		8
13	$[(PCy_3)_2(CO)(CH_3CN)_2RuH]^+BF_4^-$		0
14	$[(COD)RuCl_2]_x/HBF_4{\cdot}OEt_2$		0
15	PCy_3		0
16	$AlCl_3$		3
17	$HBF_4{\cdot}OEt_2$		4

[a]Standard reaction conditions: 3-methoxyphenol (0.50 mmol), 1-hexanal (0.50 mmol), catalyst (3 mol %), 2-propanol (0.75 mmol), 1,2-dichloroethane (1 mL), 120 °C, 12 h. [b]The product yield was determined by ^1H NMR by using hexamethylbenzene as an internal standard.

yielding the alkylation product **2a** among the screened ruthenium catalysts (entries 1 and 8). 1,2-Dichloroethane was found to be the most suitable solvent for the coupling reaction among those screened.

Having observed the promotional effect of hydrogen donors on the product formation, we next examined the additive effects on the product selectivity for the coupling reaction of 3-methoxyphenol with the branched aldehyde 2-phenyl-1-propanal (eq 2). Initially, a 1:3.5 mixture of the alkylation

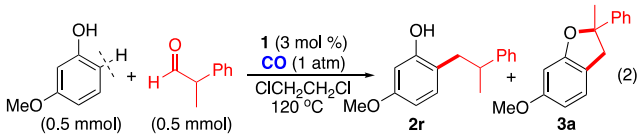

product **2r** and the benzofuran product **3a** was formed in 30% combined yield in the absence of a hydrogen source (Table 2, entry 1). As expected, the addition of H_2 (5 atm) or 2-propanol (1.5 equiv) greatly improved the product yield and selectivity for **2r** over **3a** (entries 2 and 3). Interestingly, the addition of CO (1 atm) completely reversed the product selectivity in favor of the benzofuran product **3a**, and subsequent optimization efforts have established the standard conditions for the formation of **3a** (entry 4). Other additives such as formic acid, CO_2, and olefins were found to be completely ineffective in promoting the formation of **3a** (entries 5−7). In this case, the *in situ* formed catalyst from the tetranuclear Ru−H complex with $HBF_4{\cdot}OEt_2$ was found to be substantially less effective in giving **3a** in comparison to the catalyst **1** (entry 10).

Reaction Scope. The substrate scope of the alkylation reaction was explored by using the standard conditions established in Table 1 (Table 3). Even though both H_2 and

https://doi.org/10.1021/jacs.1c06887
J. Am. Chem. Soc. 2021, 143, 13428−13440

Table 2. Additive Effects and Optimization Study for the Dehydrative Coupling of 3-Methoxyphenol with 2-Phenyl-1-propanal[a]

entry	catalyst	deviation from standard conditions	yield (**2r**:**3a**) (%)[b]
1	**1**	none	6:21
2	**1**	H_2 (5 atm)	90:5
3	**1**	2-propanol (0.75 mmol)	88:5
4	**1**	CO (1 atm)	9:89
5	**1**	HCO_2H (0.75 mmol)	0:0
6	**1**	cyclopentene (0.75 mmol)	12:50
7	**1**	CO_2(1 atm)	0:0
8	**1**	CH_3CN	0:0
9	$[(PCy_3)(CO)RuH]_4(O)(OH)_2/H^+$	H_2 (5 atm)	74:0
10	$[(PCy_3)(CO)RuH]_4(O)(OH)_2/H^+$	CO (1 atm)	15:58
11	$(PCy_3)_2(CO)RuHCl/HBF_4{\cdot}OEt_2$	CO (1 atm)	10:20
12	$RuCl_2(PPh_3)_3/HBF_4{\cdot}OEt_2$	CO (1 atm)	0:2
13	$RuCl_3{\cdot}3H_2O$	CO (1 atm)	0:0
14	$Ru_3(CO)_{12}/HBF_4{\cdot}OEt_2$	H_2 (5 atm)	21:0
15	$[(PCy_3)_2(CO)(CH_3CN)_2RuH]^+BF_4^-$	H_2 (5 atm)	0:5

[a]Standard reaction conditions: 3-methoxyphenol (0.50 mmol), 2-phenyl-1-propanal (0.50 mmol), 1,2-dichloroethane (1 mL), 120 °C, 12 h. [b]The product yield was determined by ^{1}H NMR by using hexamethylbenzene as an internal standard.

Table 3. Dehydrative C−H Coupling Reaction of Phenols with Aldehydes[a]

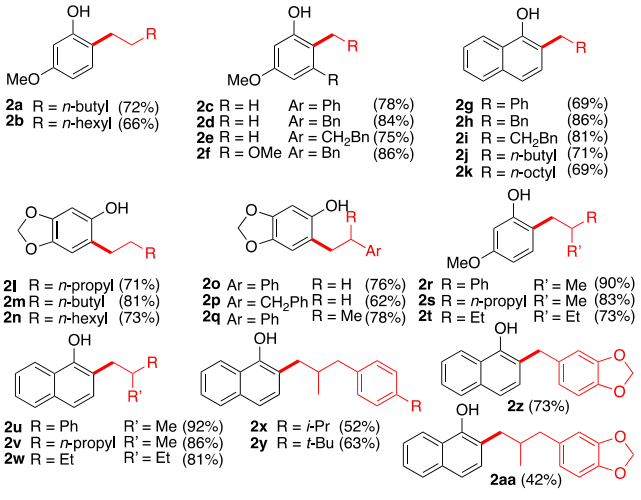

[a]Reaction conditions: phenol (1.0 mmol), aldehyde (1.0 mmol), 2-propanol (1.5 mmol), **1** (3 mol %), 1,2-dichloroethane (1 mL), 120 °C, 12 h.

2-propanol were found to be equally effective in promoting the alkylation reaction, 2-propanol was used as the hydrogen source in most cases for the sake of convenience in running the reaction. Electron-rich phenols such as 3-methoxyphenol and 3,5-dimethoxyphenol were found to be suitable substrates for the couplings with both aryl-substituted and aliphatic aldehydes to form the *ortho*-alkylated phenol products **2a−f**. The coupling of both 1-naphthol and sesamol with aryl-substituted and aliphatic linear aldehydes predictably formed the alkylation products **2g−k** and **2l−q**, respectively. The coupling of 3-methoxyphenol and 1-naphthol with *β*-substituted aldehydes formed the products **2r−t** and **2u−y** in good to excellent yields, respectively. The coupling of 1-naphthol with the biologically active aldehyde substrates piperonal and helional smoothly afforded the corresponding alkylation products **2z** and **2aa**, respectively. The coupling products were readily isolated by column chromatography on silica gel, and their structures were completely established by spectroscopic methods.

We next surveyed the substrate scope of phenols and branched aldehydes for selective formation of the 1,1-disubstituted benzofuran products **3** by using the standard conditions described in Table 2 (Table 4). Once again,

Table 4. Dehydrative C−H Coupling Reaction of Phenols with Branched Aldehydes[a]

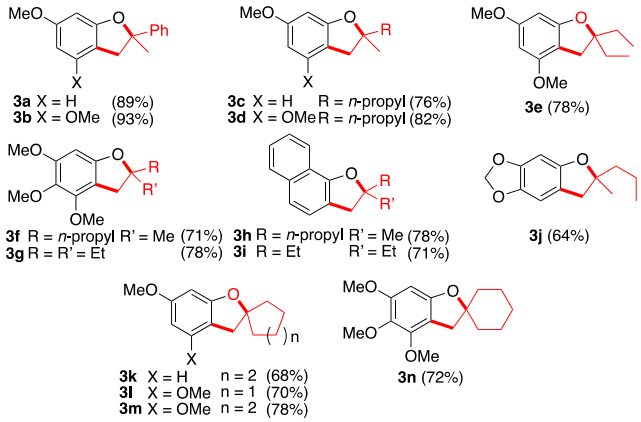

[a]Reaction conditions: phenol (1.0 mmol), aldehyde (1.0 mmol), 1,2-dichloroethane (1 mL), CO (1 atm), **1** (3 mol %), 120 °C, 12 h.

phenols with an electron-donating group such as 3-methoxyphenol and 3,5-dimethoxyphenol were found to be suitable substrates for the coupling with both aryl-substituted and aliphatic branched aldehydes in yielding the benzofuran products **3a−e**. The coupling of 3,4,5-trimethoxyphenol with branched aldehydes smoothly formed the corresponding 1,1-disubstituted benzofuran derivatives **3f,g**. The coupling of 1-naphthol and sesamol with branched aliphatic aldehydes predictably afforded the 1,1-disubstituted benzofuran products **3h,i** and **3j**, respectively, while the coupling of phenols with cyclopentanal and cyclohexanal formed the corresponding *spiro*-benzofuran products **3k−n**. In most cases, the alkylation products **2** were formed in less than 10% yields, and the analytically pure products **3** were readily isolated by silica gel column chromatography.

To further extend the synthetic utility, we explored the dehydrative coupling reaction of phenols with a variety of functionalized aldehydes. We found that the Ru−H complex **1** effectively catalyzes the dehydrative coupling of phenols with 2-hydroxybenzaldehydes to form xanthene products. Thus, the treatment of 3,5-dimethoxyphenol with salicylaldehyde in the presence of **1** (3 mol %) in 1,4-dioxane (1 mL) at 110 °C smoothly formed the xanthene product **4a** without any other detectable side products (eq 3). The addition of CO (1 atm)

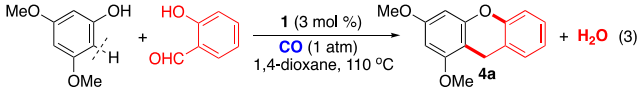

https://doi.org/10.1021/jacs.1c06887
J. Am. Chem. Soc. 2021, 143, 13428−13440

was found to promote the coupling reaction, and no external hydrogen source was necessary in this case, as the hydrogen atoms were internally furnished in forming the xanthene product **4a** and water byproduct.

The substrate scope was explored by using the optimized reaction conditions stipulated in eq 3 (Table 5). The coupling

Table 5. Dehydrative C−H Coupling Reaction of Phenols with Salicylaldehydes[a]

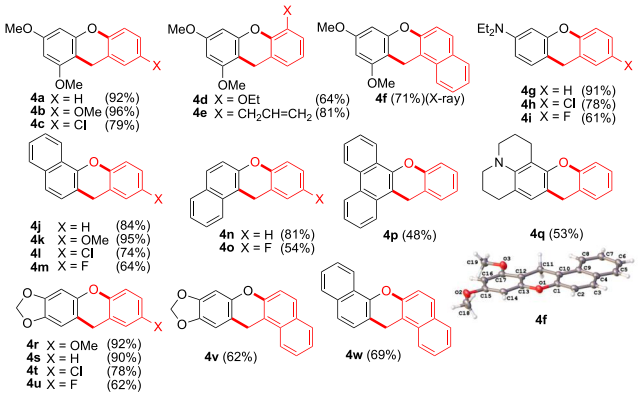

[a]Reaction conditions: phenol (1.0 mmol), aldehyde (1.0 mmol), **1** (3 mol %), 1,4-dioxane (1 mL), 110 °C, 12−16 h.

of 3,5-dimethoxyphenol with both electron-rich and electron-poor salicylaldehydes readily formed the xanthene products **4a−f**. The coupling of 1-naphthol with salicylaldehydes formed the products **4j−m** from the C−H coupling at the C2 position, while the analogous coupling of 2-naphthol formed the products **4n,o** resulting from cyclization at the C1 position. The coupling of polycyclic substrates 9-phenanthrol and 8-hydroxyjulolidine with salicylaldehydes selectively formed the polyaromatic xanthene derivatives **4p,q**, respectively. The coupling of sesamol with salicylaldehyde and with 2-hydoxonapthaldehyde predictably afforded the corresponding products **4r−v**. All of these xanthene products were readily isolated after silica gel column chromatographic separation, and their structures were completely established by spectroscopic methods. One of the characteristic spectroscopic features of these xanthene products **4** is the observation of a methylene peak at around δ 4.0 ppm by ^{1}H NMR. The structure of **4f** was also determined by X-ray crystallography.

Deuterium Labeling Study. We performed the following set of kinetic experiments to probe the mechanism of the C−H alkylation reaction. First, we selected the coupling reaction of 3-methoxyphenol with a deuterated benzaldehyde to examine the H/D exchange pattern (Scheme 1). Thus, the mixture of 3-methoxyphenol (1.0 mmol) with benzaldehyde-α-*d* (95% D,

Scheme 1. Deuterium Labeling Study

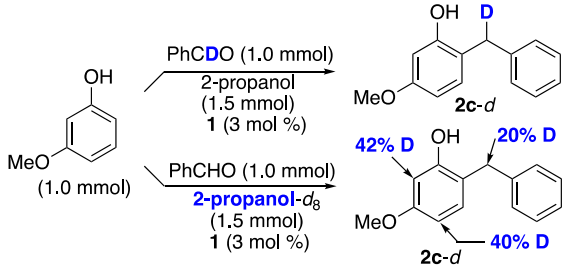

1.0 mmol) and 2-propanol (1.5 mmol) in the presence of complex **1** (3 mol %) in 1,2-dichloroethane (1 mL) was heated at 120 °C for 12 h. The isolated product **2c**-*d* showed ca. 50% of the deuterium on the α-CH_2 position without any significant deuterium scrambling to other arene positions, as analyzed by ^{1}H and ^{2}H NMR spectroscopy. In contrast, the product **2c**-*d* isolated from the analogous treatment of 3-methoxyphenol (1.0 mmol) with benzaldehyde (1.0 mmol) and 2-propanol-d_8 (99.5% D, 1.5 mmol) showed only 20% of the deuterium on the α-CH_2 group along with significant deuterium incorporations at both the *ortho* and *para* arene positions (40−42% D). In a control experiment, the treatment of isolated **2c** with 2-propanol-d_8 and **1** (3 mol %) at 120 °C for 12 h did not lead to any significant deuterium exchange to the α-CH_2 position but rather to the *ortho* and *para* arene positions (36−37% D). These results clearly showed that the aldehydic C−H bond was not broken during the coupling reaction and that the significant deuterium incorporation at the α-CH_2 group resulted from an H/D exchange with 2-propanol-d_8. The H/D exchange to *ortho* and *para* arene positions can readily be explained via a separate arene C−H metalation process, which has been shown to be rapid and reversible in transition-metal-catalyzed arene C−H coupling reactions.[18]

Hammett Study. The rate of the alkylation reaction of 3-methoxyphenol (1.0 mmol) with *para*-substituted benzaldehydes *p*-X-C_6H_4CHO (1.0 mmol) (X = OMe, Me, H, F, Cl, CF_3) in the presence of 2-propanol (1.5 mmol) and **1** (3 mol %) in 1,2-dichloroethane-d_4 (1.2 mL) was measured by using an NMR spectrocopic method (eq 4). The appearance of the

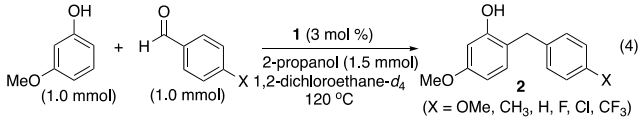

product peaks was normalized against an internal standard (hexamethylbenzene) in 20 min intervals, and the k_{obs} value of each catalytic reaction was determined from a first-order plot of $-\ln[(\text{3-methoxyphenol})_t/(\text{3-methoxyphenol})_0]$ vs time. The Hammett plot was constructed from $\log(k_X/k_H)$ vs σ_p, which showed a V-shaped linear correlation pattern (Figure 1). A highly negative linear slope was observed from the aldehydes with an electron-donating group (ρ = −2.9 ± 0.1; X = OMe, Me, H), while a positive slope resulted from the aldehydes with

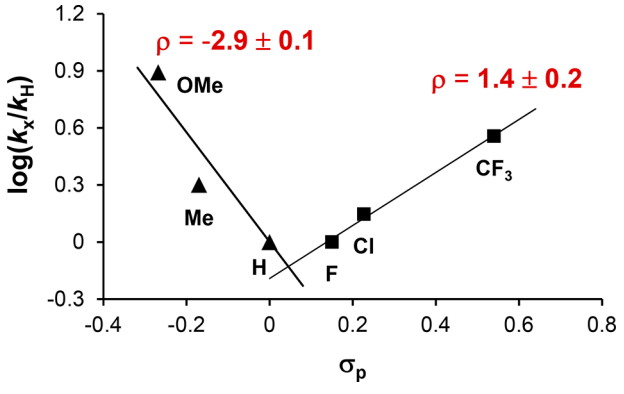

Figure 1. Hammett plot from the coupling reaction of 3-methoxyphenol with *p*-X-C_6H_4CHO (X = OMe, Me, H, F, Cl, CF_3).

https://doi.org/10.1021/jacs.1c06887
J. Am. Chem. Soc. 2021, 143, 13428−13440

an electron-withdrawing group (ρ = +1.4 ± 0.2; X = F, Cl, CF_3).

A V-shaped Hammett correlation has generally been attributed to a change in the reaction mechanism.[19] Abu-Omar and co-workers reported a V-shaped Hammett plot in the hydrogen atom transfer reaction of Mn-imido complexes with *para*-substituted phenols, from which two distinct hydrogen transfer mechanisms have been inferred.[19a] While studying oxygen atom transfer reaction of Mn-oxo complexes, Goldberg and co-workers observed a similar V-shaped Hammett correlation pattern from the reaction with *para*-substituted benzothioethers.[19b] We previously observed a V-shaped Hammett correlation from the ruthenium-catalyzed hydrogenolysis of ketones, in which a change in the electronic nature of the *para*-substituted phenolic ligand has been found to alter the kinetics of hydrogen addition and C−O bond hydrogenolysis steps.[20]

Deuterium and Carbon Kinetic Isotope Effects. To probe the electronic effect of aldehyde substrates on the reaction mechanism, we next measured the deuterium isotope effect of 2-propanol vs 2-propanol-d_8 from the coupling reaction of 3-methoxyphenol with a series of *para*-substituted benzaldehydes (eq 5). In a parallel reaction setting, the rate of

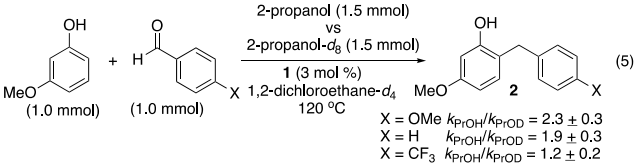

3-methoxyphenol with *p*-X-C_6H_4CHO (X = OMe, H, CF_3) and 2-propanol (1.5 equiv) or 2-propanol-d_8 (1.5 equiv) in the presence of **1** (3 mol %) in 1,2-dichloroethane-d_4 (1.0 mL) at 120 °C was measured by monitoring the appearance of product signals by ^{1}H NMR. The k_{obs} value was determined from a first-order plot of $-\ln[(\text{3-methoxyphenol})_t/(\text{3-methoxyphenol})_0]$ vs time, and k_H/k_D was calculated from the slope for each case (Figure 2). A relatively high normal deuterium isotope effect was observed with the benzaldehyde with an electron-releasing group *p*-OMe-C_6H_4CHO (k_H/k_D = 2.3 ± 0.3) and for benzaldehyde (k_H/k_D = 1.9 ± 0.3), while a negligibly small deuterium isotope effect was measured for the benzaldehyde with an electron-withdrawing group *p*-CF_3-C_6H_4CHO (k_H/k_D = 1.2 ± 0.3). The pronounced normal deuterium isotope effect for both benzaldehyde and 4-methoxybenzaldehyde implies that the hydrogen transfer step may be turnover-limiting for these cases. On the other hand, the negligibly small deuterium isotope effect from the coupling of the benzaldehyde with an electron-withdrawing group *p*-CF_3-C_6H_4CHO suggests that hydrogen transfer is not the turnover-limiting step. Both the deuterium effect and Hammett data indicate that the rate of the hydrogen transfer step is strongly influenced by the electronic nature of the aldehyde substrates. We measured the rates in the first 2 h of reaction time because a relatively high catalytic activity of **1** was observed initially, as indicated by a relatively high turnover frequency in the first hour (TOF 10−15 h^{-1}), but its activity noticeably decreased after the second hour (TOF < 5 h^{-1}). The depreciation of catalytic activity can be attributed to both the product inhibition as well as the decomposition of the Ru catalyst.

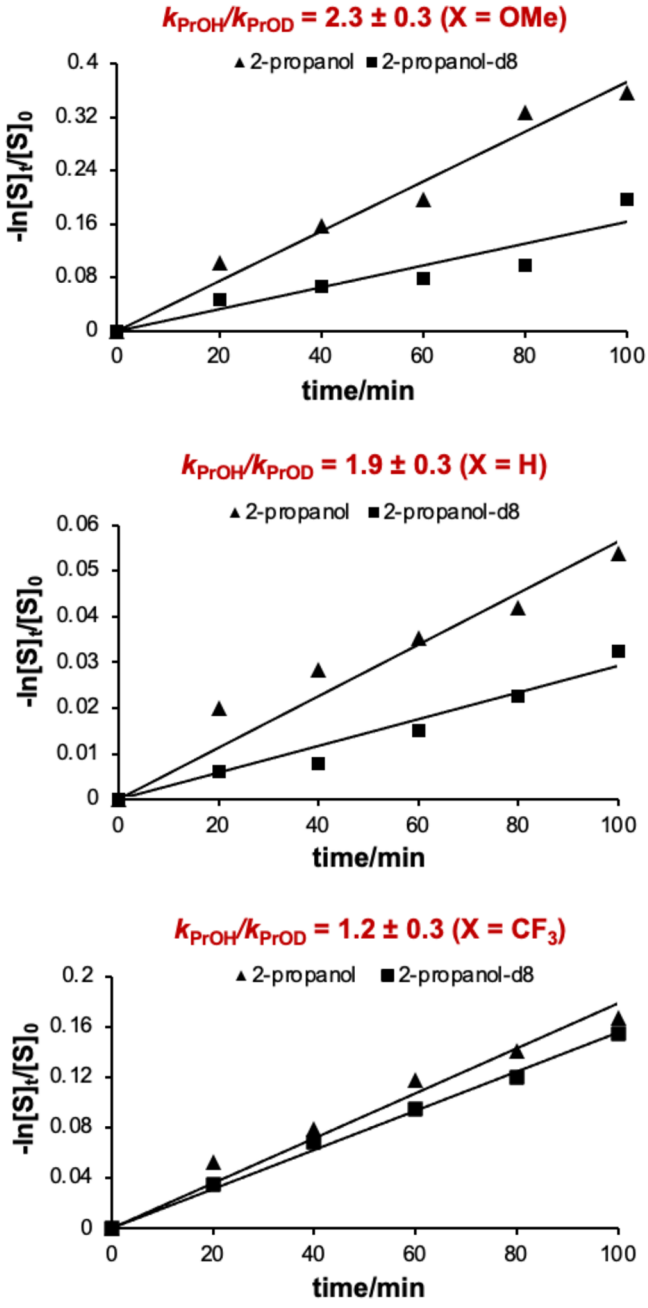

Figure 2. First-order plots from the reaction of 3-methoxyphenol with *p*-X-C_6H_4CHO (X = OMe, H, CF_3) and 2-propanol vs 2-propanol-d_8. S = 3-methoxyphenol.

The deuterium isotope effect and Hammett data suggest that either the C−C bond formation or the hydrogen transfer step could be the rate-determining step depending on the electronic nature of the aldehyde substrates. To further discern the turnover-limiting step of the coupling reaction, we measured the carbon isotope effect from the coupling reaction of 3-methoxyphenol with *para*-substituted benzaldehydes *p*-X-C_6H_4CHO (X = OMe, H, CF_3) by employing Singleton's high-precision NMR technique (Scheme 2).[21] The high-conversion samples of **2bb** (X = OMe), **2c** (X = H), and **2cc** (X = CF_3) were obtained from three separate treatments of 3-methoxyphenol (1.0 mmol), *p*-X-C_6H_4CHO (1.0 mmol), 2-propanol (1.5 mmol), and complex **1** (3 mol %) in 1,2-dichloroethane (1 mL) at 120 °C for 12 h (83%, 88%, and 89%

https://doi.org/10.1021/jacs.1c06887
J. Am. Chem. Soc. 2021, 143, 13428−13440

Scheme 2. Carbon Kinetic Isotope Effects from the Coupling of 3-Methoxyphenol with *p*-X-C_6H_4CHO (X = OMe, H, CF_3)

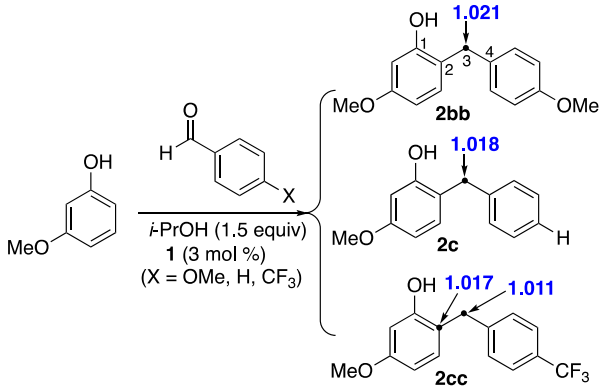

conversion, respectively). The low-conversion samples were similarly isolated from three separate reactions of 3-methoxyphenol (5.0 mmol), *p*-X-C_6H_4CHO (5.0 mmol, X = OMe, H, CF_3), 2-propanol (1.5 equiv), and complex **1** (3 mol %) in 1,2-dichloroethane (3.5 mL) after 20 min of the reaction time (15%, 19%, and 19% conversion, respectively).

For the coupling reaction of an electron-rich *p*-OMe-C_6H_4CHO, the most pronounced carbon isotope effect was observed on the benzylic carbon of the product **2bb** when the ^{13}C ratio of the product from a high conversion was compared with the sample obtained from a low conversion (^{13}C(average 83% conversion)/^{13}C(average 15% conversion) at C(3) = 1.021(3); average of three runs) (Table S4 in the Supporting Information).[22] Similar results were obtained from the product **2c** (^{13}C(average 88% conversion)/^{13}C(average 19% conversion) at C(3) = 1.018(1); average of three runs). In contrast, the most prominent carbon isotope effect was observed on both *ortho* arene and benzylic carbons of **2cc** from the coupling reaction of an electron-deficient *p*-CF_3–C_6H_4CHO (^{13}C(average 89% conversion)/^{13}C(average 19% conversion) at C(2) = 1.017(3) and at C(3) = 1.011(2); average of three runs) (Table S5 in the Supporting Information). The observation of a carbon isotope effect suggests that the benzylic carbon C(3) is somehow involved in the turnover-limiting step for the electron-rich aldehydes 4-methoxybenzaldehyde and benzaldehyde. On the other hand, the observation of a carbon isotope effect on both the *ortho* arene and benzylic carbons C(2) and C(3) for the reaction of electron-poor 4-trifluorobenzaldehyde is consistent with C–C bond formation as the rate-limiting step. Overall, the carbon isotope effect results corroborate both the deuterium isotope effect studies and the Hammett data that the electrophilic nature of the aldehyde substrate plays a critical role in facilitating the rate of the alkylation reaction.

Spectroscopic Detection of Catalytically Relevant Species. We pursued the detection of catalytically relevant species by using NMR spectroscopic techniques. A stoichiometric reaction mixture containing complex **1** (0.20 mmol), 3-methoxyphenol (0.40 mmol), benzaldehyde (0.40 mmol), and 2-propanol (0.40 mmol) was dissolved in CD_2Cl_2 (0.5 mL) in a resealable NMR tube (Scheme 3). The reaction tube was immersed in an oil bath set at 120 °C and was taken out periodically to record the NMR spectra. In the ^1H NMR, a set of new doublets rapidly appeared at δ −10.8 (d, J_{PH} = 27.9 Hz) and −11.4 (d, J_{PH} = 26.2 Hz) ppm immediately after heating

Scheme 3. Detection of Catalytically Relevant Species from the Reaction of 1 with 3-Methoxyphenol and Benzaldehyde

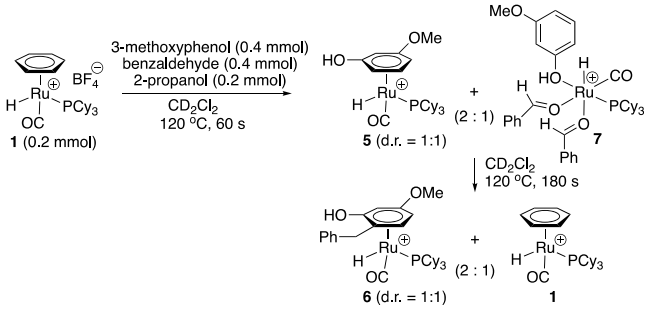

just for 10 s at 120 °C, which were assigned to a diastereomeric mixture of the phenol-coordinated Ru–H complex **5** (Figure 3). Additional heating for 60 s at 120 °C resulted in the

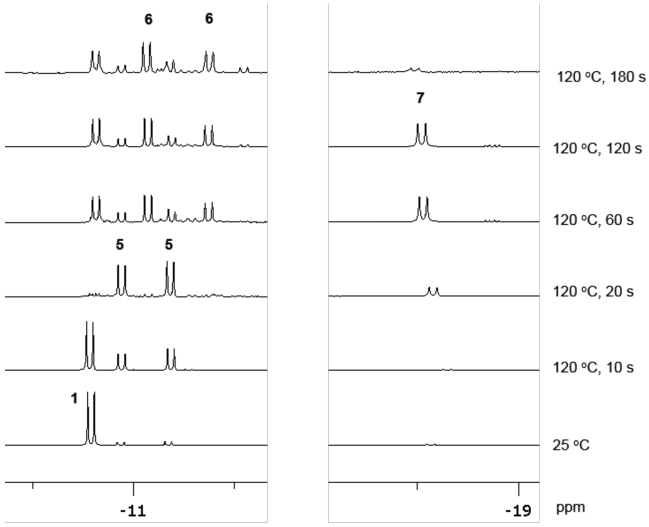

Figure 3. Partial ^1H NMR spectra obtained from the reaction of **1** with 3-methoxyphenol and benzaldehyde.

appearance of a new set of doublets at δ −11.1 (d, J_{PH} = 27.7 Hz) and −11.7 (d, J_{PH} = 28.4 Hz) ppm that were formed at the expense of signals from both **1** and **5**. These new doublet peaks were assigned to a diastereomeric mixture of the product-coordinated Ru–H complex **6**. While the NMR spectral data of these Ru–H complexes **5** and **6** match well with the independently generated spectra (Figures S10 and S11 in the Supporting Information), we could not unambiguously assign their structures because we could not obtain these complexes in their pure form.

Interestingly, another set of new Ru–H peaks began to appear at δ −18.8 (d, J_{PH} = 32.1 Hz) after 20 s at 120 °C and reached its maximum intensity after heating for 120 s. We recognized that a noticeably upfield shifted Ru–H peak is in the region typically seen for oxygen-coordinated cationic Ru–H complexes.[23] Since both benzaldehyde and phenol substrates as well as 2-propanol could reversibly coordinate to the Ru center, we could not assign the structure of the complex solely on the basis of the spectroscopic data. We performed DFT calculations to determine which of these oxygen ligand combinations would result in the most stable configuration. The calculations showed that the Ru–H complex with the phenol and two *trans*-coordinated

https://doi.org/10.1021/jacs.1c06887
J. Am. Chem. Soc. 2021, 143, 13428–13440

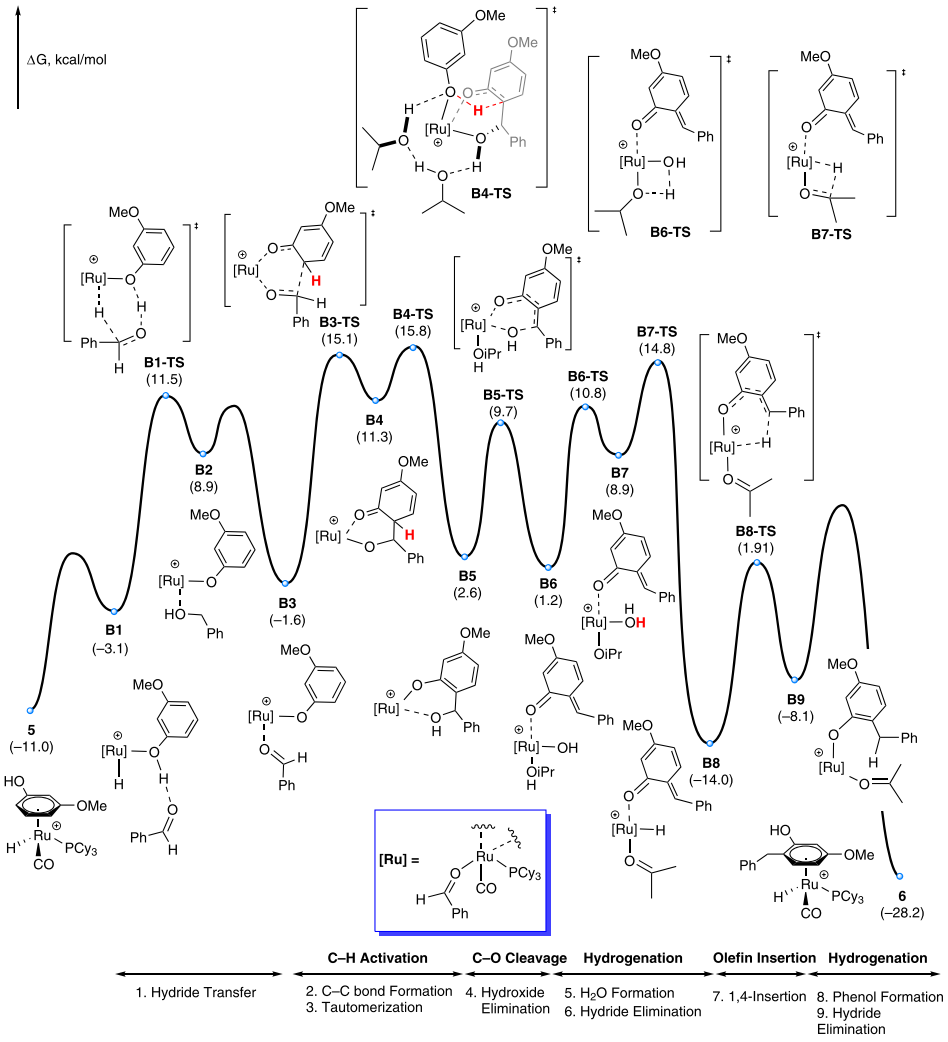

Figure 4. Gibbs free energy profile for the coupling reaction of 3-methoxyphenol with benzaldehyde (kcal/mol). Thermodynamic and solvation contributions assume ideal and standard conditions.

benzaldehyde groups has the lowest energy out of the possible structures, and we tentatively assigned the Ru−H peak as that of complex **7** on the basis of the DFT analysis (*vide infra*).[24] Eventually, these Ru−H peaks reached a steady state after heating for 180 s at 120 °C and gradually disappeared upon further heating for about 5 min. However, the Ru−H peaks remain unchanged when the sample was stored at room temperature, and no free phosphine or other phosphine-containing species were detected by $^{31}P\{^{1}H\}$ NMR.

DFT Computational Study. We performed density functional theory (DFT) calculations to validate the experimental data and to attain deeper mechanistic insights into the alkylation reaction. We initially profiled a number of plausible catalytic pathways and successfully identified a low-energy pathway for the complete catalytic cycle for the coupling reaction of 3-methoxyphenol with benzaldehyde, as illustrated in Figure 4. Initially, the catalyst **5** is activated by reacting with the aldehyde substrate, featuring a concerted hydride transfer from Ru to the carbonyl carbon and proton transfer from phenol to the carbonyl oxygen. This reaction step has an overall barrier of 22.5 kcal/mol, and the intermediate **B2**, a Ru-phenoxide complex with a pendant benzyl alcohol, is 19.9 kcal/mol less stable than the initial catalyst **5**, rendering the catalyst activation step highly reversible.

The pendant benzyl alcohol is fairly labile with a dissociation energy of −2.2 kcal/mol. Thus, another benzaldehyde substrate can readily displace the benzyl alcohol from the intermediate **B2** and release an additional 10.5 kcal/mol of Gibbs free energy. Note that the resulting intermediate **B3** possesses two benzaldehyde molecules, as the Ru center preferentially binds benzaldehyde over other OH-functionalized compounds in an η^1 fashion. As illustrated in Figure 5, the HOMO π-orbital of **B3** is delocalized across the Ru-alkoxy moiety, whereas the LUMO predominantly has π^*(C═O) contributions from two benzaldehyde molecules. The HOMO to LUMO electron transfer process facilitates the insertion of the benzaldehyde substrate to the Ru-aryloxo moiety of **B3**. These calculated results are consistent with the spectroscopic detection of the Ru−H complex **7**, in which the conversion of π to oxygen coordination mode of the phenol ligand allows the coordination of two benzaldehyde substrates. A noticeably upfield shifted Ru−H peak of **7** in ^{1}H NMR data supports an increase in basicity due to the coordination of benzaldehyde oxygen atoms, and the catalytically active Ru-phenoxo species **B3** would be formed from **B1** via an H_2 elimination (from the phenol proton and the metal hydride).

Traversing the transition state **B3-TS** furnishes the **B4** intermediate at 22.3 kcal/mol above the catalytic resting state

https://doi.org/10.1021/jacs.1c06887
J. Am. Chem. Soc. 2021, 143, 13428−13440

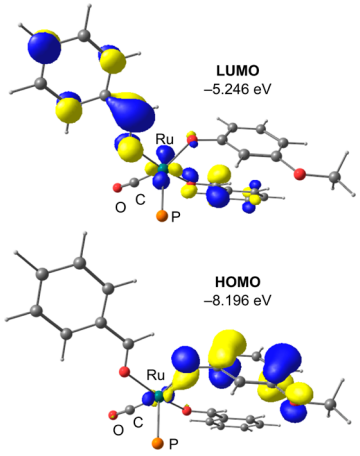

Figure 5. Frontier orbitals of **B3** illustrated with an isodensity of 0.5 au. Cyclohexyl groups are omitted for clarity.

5. Although the resulting intermediate is relatively unstable, its tautomerization will push the reaction forward to the 8.7 kcal/mol more stable intermediate **B5** with a bis-2-hydroxy-(phenyl)methyl phenolate ligand. Mechanistically, the tautomerization can be understood as a series of proton transfer steps between each tautomer assisted by proton transfer agents.[25] Computational models often refer to the mechanism as "proton shuttling" that can be facilitated by either solvent molecules or other external agents. Among the possible facilitators, the phenol group offers the lowest energy pathway from two participating additional 2-propanol molecules with an overall barrier of 26.8 kcal/mol. Similar intramolecular proton transfer processes with other viable candidates have notably higher barriers, as illustrated in Figure S16 in the Supporting Information.

We explored an alternative mechanistic pathway to intermediate **B5**, as illustrated in Figure S10 in the Supporting Information. This pathway involves the formation of an *ortho*-metalated Ru-aryl species due to arene C−H activation and dehydrogenation steps (path A). On the basis of both experimental and computational data, we previously showed that the dehydrative C−H coupling of phenol with ketones occurs through an *o*-C−H metalation leading to (*Z*)-olefin products.[17] However, in the current case, such a pathway appears to be highly unlikely because the concerted C−H bond activation via σ-bond metathesis has a very high energy barrier ($\Delta G^{\ddagger}$ = 47.7 kcal/mol, Figure S10). In related Ru(II)-catalyzed olefin hydroarylation reactions, Cundari and co-workers suggested that the barrier to the σ-bond metathesis reaction can vary from 31 to 43 kcal/mol depending on the Ru-bound ancillary ligands.[26] Notwithstanding the catalysts' differences, the current DFT results are consistent with the high-barrier regime of Cundari's previous studies.[26] Thus, we conclude that the initial dehydrogenation of the phenol-coordinated complex **5** is an essential catalyst initiation step leading to the Ru-phenoxo species **B3** (path B), and this path is also supported by our previously demonstrated Ru-phenoxo complex as the key species for the hydrogenolysis of carbonyl compounds.[20] The subsequent coupling of the Ru-phenoxo species with another aldehyde substrate would furnish the observed alkylation product **2**, as described below.

After the C−H activation via electrophilic aromatic substitution and tautomerization, the catalytic cycle continues on with the hydroxide elimination from the bis-2-hydroxy-(phenyl)methyl phenolate ligand of the **B5** intermediate. This transformation is best described as a hydroxide transfer from the benzylic position, resulting in the formation of *o*-methide quinone and a Ru−OH moiety. The transition state **B5-TS** is found at 20.7 kcal/mol and leads to intermediate **B6** at 12.2 kcal/mol (Figure 6). In general, the methide quinone is highly

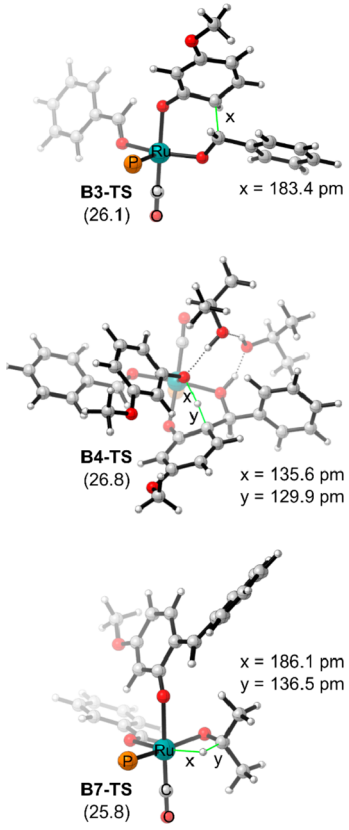

Figure 6. Transition-state geometries of C−C bond formation (**B3-TS**), tautomerization (**B4-TS**), and hydride elimination (**B7-TS**) steps. Cyclohexyl groups are omitted for clarity. Gibbs energies, in kcal/mol, are relative to the catalytic resting state **5**.

electrophilic,[27] and a back-reaction to **B5** can be expected due to the (re)capture of the hydroxide by *o*-methide quinone. A stepwise hydrogenation of the **B6** intermediate by the pendant 2-propanol drives the catalysis forward. The first step of the hydrogenation involves a proton transfer from 2-propanol to the Ru−OH group, forming aqua and 2-propoxy ligands. As the aqua ligand dissociates, the β-hydride elimination of the isopropoxy ligand may generate the **B8** intermediate, which is another Ru−H species. The β-hydride elimination has a barrier of 25.8 kcal/mol and is therefore easier than the tautomerization, as illustrated in Figure 4. Given that there are several possible reaction trajectories involving various proton-transfer agents, as shown in Figure S16 in the Supporting Information, it is very likely that the tautomerization of **B4** is rate limiting. Furthermore, the Ru−H intermediate **B8** is 3.0 kcal/mol lower in energy than **5**, indicating that this intermediate is not in a reversible equilibrium with **5**. The ensuing hydride transfer to the *o*-methide quinone moiety has a barrier of 15.9 kcal/mol, and the reaction proceeds further with the hydrogenation of the resulting intermediate **B9**. The second hydrogenation will require another 2-propanol to form the intermediate **6** with the desired alkylation product. The Ru complex **6** was detected by

https://doi.org/10.1021/jacs.1c06887
J. Am. Chem. Soc. 2021, 143, 13428−13440

NMR spectroscopic methods, and our DFT calculations found the alkylation product to be at −13.2 kcal/mol. The regeneration of **5** will occur when the 3-methoxyphenol substrate displaces the desired product from the Ru−H complex **6** and releases an additional 1.1 kcal/mol of Gibbs free energy.

Electronic Effect of the Aldehyde Substrate. Both the kinetic isotope effect and Hammett data showed that the electronic nature of the aldehyde substrate affects the rate of the reaction and, more importantly, alters the rate-limiting step. To better understand these experimental data, we re-examined the proposed mechanism computationally with the *para*-substituted benzaldehyde substrates *p*-X-C_6H_4CHO (X = OMe, CF_3). We observed a significant destabilizing effect by the *p*-CF_3 substituent on the C−C bond forming transition state, as the C−C bond formation barrier is increased by 3.1 kcal/mol (Figure 7). In comparison, the *p*-methoxy substituent

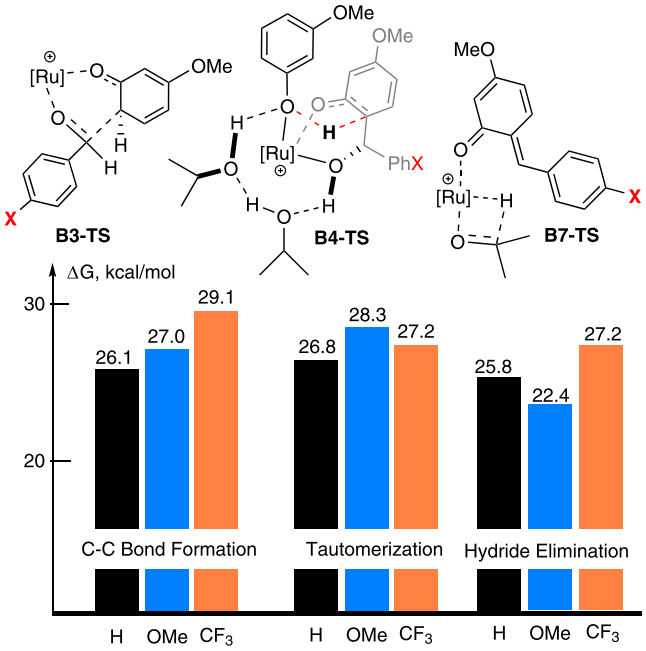

Figure 7. Barriers of the C−C bond formation, tautomerization, and hydrogenation with *para*-substituted benzaldehyde substrates (*p*-X-C_6H_4CHO, X = OMe, CF_3). Gibbs energies, in kcal/mol, are relative to the Ru−H complex **5**.

exhibited a relatively small destabilizing effect, giving an increase of only 0.9 kcal/mol on the barrier. A natural population analysis (NPA) revealed ∼0.36e charge transfer from the aryloxy ligand to the benzaldehyde at the C−C bond forming transition state when the *p*-CF_3 substituent is present. The charge transfer is slightly smaller in comparison to those of the unsubstituted benzaldehyde and 4-methoxybenzaldehyde, which are 0.43e and 0.44e, respectively. Although the charge-transfer data correlate with the increased barrier caused by the *p*-CF_3 substituent, the trend is counterintuitive because, intuitively, the more electrophilic *p*-CF_3-C_6H_4CHO substrate would be expected to be more effective in promoting the electrophilic attack to the Ru-aryloxo group.

The HOMOs of the reactant complexes reveal unanticipated shifts in energies due to the *para* substituents of benzaldehyde. With the *p*-CF_3-C_6H_4CHO substrate, the HOMO energy decreases by 0.23 eV relative to the unsubstituted benzaldehyde, indicating that the aryloxy ligand becomes less nucleophilic. This decrease in nucleophilicity is the reason for a 3.1 kcal/mol increase in the C−C bond formation barrier. Thus, in agreement with the ^{13}C kinetic isotope data, the calculations predict the C−C bond formation step to be associated with the highest barrier for the *p*-CF_3-C_6H_4CHO substrate. Conversely, the HOMO energy increases by 0.22 eV with *p*-OMe-C_6H_4CHO, revealing an increase in the nucleophilic character of the aryloxy ligand. Despite the higher nucleophilicity, the barrier for C−C bond formation also increases, albeit only by 0.9 kcal/mol, relative to the unsubstituted benzaldehyde largely because *p*-OMe-C_6H_4CHO is a relatively weak electrophile.

The highest computed barriers for *p*-CF_3-C_6H_4CHO and *p*-OMe-C_6H_4CHO substrates are 29.1 kcal/mol (C−C bond formation step) and 28.3 kcal/mol (tautomerization step), which compare well with the barriers obtained from the first-order rate constants, 31.4 and 30.8 kcal/mol, respectively (Figure 7). The computational results qualitatively explain the origin of two different rate-determining steps for these substrates: the tautomerization rate-limiting step for the electron-rich *p*-OMe-C_6H_4CHO substrate and the C−C bond formation rate-limiting step for the electron-poor *p*-CF_3-C_6H_4CHO substrate. However, the DFT computational data fail to portray the general trend observed from the experimental Hammett plot, in which the unsubstituted benzaldehyde had the lowest rate among the substituted benzaldehydes. Instead, the tautomerization barrier for unsubstituted benzaldehyde of 26.8 kcal/mol is the lowest value among these aldehydes. To resolve this apparent disagreement between the experimental results and the computed values, we compared the energies for these intermediate species by using several different DFT methods, including M06-D3, PBE0-D3, M06L-D3, TPSSh-D3, and wB97x-D3 (Tables S8−S13). While most of these DFT methods correctly predicted the rate-limiting step for both unsubstituted and *para*-substituted benzaldehydes, none of the methods correctly corroborated the experimentally observed reactivity trend for the aldehydes *p*-X-C_6H_4CHO (X = OMe > CF_3 > H). Since several elementary steps separate between the transition states **B3-TS** (C−C bond formation) and **B4-TS** (tautomerization) and the catalytic resting state **5**, we recognize that any of these steps could significantly contribute to the overall kinetics for these aldehyde substates. A comprehensive characterization of the equilibrium species as well as subsequent microkinetic modeling studies may be needed to better model the experimentally observed reactivity pattern for these *para*-substituted benzaldehydes.

Proposed Mechanism. We compiled a reasonable mechanism for the catalytic alkylation of phenol with benzaldehyde on the basis of these experimental and computational results, as illustrated in Scheme 4. We propose that the catalytically active Ru−H complex **5** is initially formed from the arene exchange reaction of **1** with the phenol substrate, and in support of this notion, we have been able to detect complex **5** spectroscopically. The spectroscopic detection and the DFT-aided structural elucidation of the phenol-coordinated Ru−H species **7** also provided strong evidence for the generation of the Ru-aryloxy complex **8** from the dehydrogenation of **7**.

The DFT calculations revealed that an electrophilic substitution of the aldehyde via the formation of Ru-phenoxo complex **8** has a considerably lower energy pathway than the

https://doi.org/10.1021/jacs.1c06887
J. Am. Chem. Soc. 2021, 143, 13428−13440

Scheme 4. Proposed Mechanism of the Coupling Reaction of Phenol with *para*-Substituted Benzaldehyde

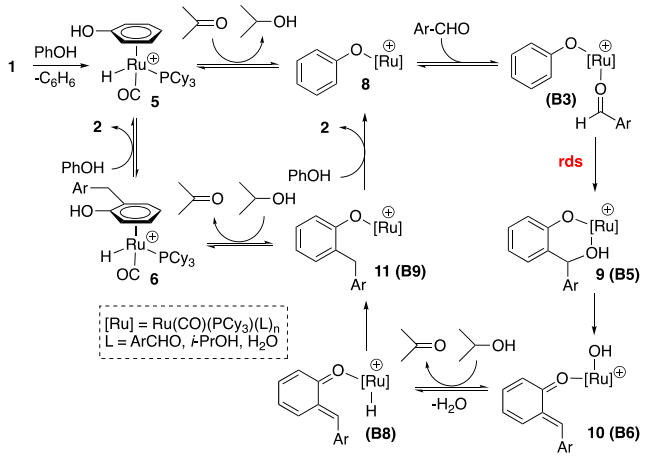

alternative *ortho*-C−H metalation and aldehyde insertion pathway. The DFT calculations further uncovered a detailed mechanistic rationale for the C−C bond formation as a two-step process (**B3** to **B5**): the first step involves an electrophilic addition of the aldehyde substrate to the *o*-arene carbon of the coordinated phenoxo ligand and the second step a stepwise proton and hydride transfer and phenoxy−dienone tautomerization to form the hydroxy-coordinated Ru-aryloxo species **B5**. The DFT calculations also revealed a detailed mechanistic rationale for the C−O bond hydrogenolysis process, which first involves the hydroxide elimination in forming the Ru-hydroxo species **10** (**B6**), followed by a series of stepwise proton and hydride transfer and water elimination steps in forming the elaborated Ru-aryloxo species **11** (**B9**). Finally, the proton exchange reaction of **11** (**B9**) with another phenol substrate would form the product **2** with the regeneration of the Ru-phenoxo species **8**. In light of the spectroscopic detection of **5** and **6**, an alternative pathway involving the transfer hydrogenation of **11**, which would form the product-coordinated Ru−H complex **6**, and the subsequent arene ligand exchange reaction with another phenol substrate could give the product **2** with the regeneration of the Ru−H complex **5**. However, we believe that the former route via the protonolysis of Ru-phenoxo species **8** is the dominant pathway under the catalytically relevant conditions, given that the binding affinity of the phenol group has been found to be considerably higher than that of 2-propanol and the protonolysis rate of transition-metal-phenoxo complexes has been known to be quite fast even at ambient temperature.[28]

The V-shaped Hammett correlation data suggested that the rate of the energetically demanding and turnover-limiting step is strongly dependent on the electronic nature of the aldehyde substrates. The DFT study uncovered a detailed mechanistic rationale for the turnover-limiting step for the alkylation reaction that the C−C bond formation step has the highest energy barrier for the electron-deficient aldehyde *p*-CF_3-C_6H_4CHO, while the tautomerization step, which involves a proton transfer from the C(2) position of the Ru-aryloxide, is the most energetically demanding step for the electron-rich aldehyde *p*-OMe-C_6H_4CHO. The appearance of a deuterium isotope effect from tautomerization step for electron-rich benzaldehydes was somewhat difficult to rationalize initially. In light of the experimental observation of a facile hydrogen−deuterium exchange to the *o*-C−H phenol substrate, as shown in Scheme 1, we estimated that more than 40% of the initial *o*-C−H arene hydrogen would be deuterated from the hydrogen−deuterium exchange process. We presume that the tautomerization step should involve about 40% of deuterium transfer, which is resulted from a hydrogen−deuterium exchange at the *ortho* arene position of the Ru-aryloxy intermediate **B4**. To support this hypothesis, we computed the deuterium kinetic isotopic effect for the unsubstituted benzaldehyde, which led to a normal deuterium isotopic effect of k_H/k_D = 3.43 for the tautomerization step. In contrast, an analogous computation of the hydrogenation step results in an inverse isotope effect of k_H/k_D = 0.52, indicating an inversion in the reaction rate due to the presence of deuterium in the transition state for the hydrogenation step. Previously, Casey and co-workers observed a normal deuterium isotopic effect of 2.1 in the transfer hydrogenation of carbonyl compounds, which was rationalized by invoking an outer-sphere mechanism via a concerted hydride and proton transfer for the hydrogenation step.[29] In our case, a similar outer-sphere mechanism has been found to have 8.2 kcal/mol higher energy barrier than the stepwise mechanism via **B7-TS** (Figure S21). Thus, DFT calculations indicated that a normal kinetic isotopic effect must have originated from the tautomerization step. In contrast to electron-rich benzaldehydes, the C−C bond formation has become the rate-determining step for the electron-deficient aldehyde *p*-CF_3-C_6H_4CHO, due to its substantially increased energy barrier. Regardless, both the C−C bond formation and tautomerization steps constitute a broader C−H activation mechanism, which is reminiscent of a classical electrophilic aromatic substitution reaction (S_EAr). Simmons and Hartwig provided cautionary comments on interpreting kinetic isotope data for C−H bond activation reactions without an accompanying computational study,[30] but our combined experimental and computational data delivered a detailed, coherent picture on the C−C bond formation step of the reaction.

On a practical note, the catalytic method can modulate the product selectivity by controlling the hydrogen concentration so that the formation of the 2-alkylphenol product is favored under hydrogen-rich conditions, whereas the benzofuran product is favored under hydrogen-deficient conditions. We observed a relatively high catalytic activity of **1** initially, but its activity was noticeably decreased after the first hour. Such a depreciation of catalytic activity after the first hour can be mostly attributed to a steady deactivation of the Ru catalyst. As a result, the catalytic reaction was typically run for 12 h in order to obtain the maximum product yield. A more robust Ru catalyst would be needed to overcome one of the major limitations of the short catalyst lifetime.

■ CONCLUSION

In summary, we have successfully developed a novel Ru-catalyzed dehydrative C−H coupling method of phenols with aldehydes as an efficient synthetic strategy for the synthesis of a diverse array of substituted phenol and benzofuran products. The direct C−H coupling reaction of phenols with 2-hydroxyarylaldehydes led to the formation of synthetically useful xanthene derivatives. The observed kinetic isotope effects as well as V-shaped Hammett correlation data showed a strong electronic dependence of the benzaldehyde substrates on the rate of the coupling reaction. A DFT computational study provided a relatively low energy pathway via the

https://doi.org/10.1021/jacs.1c06887
J. Am. Chem. Soc. 2021, 143, 13428−13440

formation of a Ru-aryloxo complex that features the electrophilic addition of aldehyde, hydroxide elimination, and subsequent transfer hydrogenation steps. The DFT study also revealed intricate and counterintuitive mechanistic insights into the role of aldehyde substrates in influencing the rate of the catalytic reaction. On consideration of both the synthetic and environmental benefits, the catalytic coupling method has a number of salient features in that it employs readily available aldehyde substrates and does not employ any reactive reagents or produce any harmful byproducts. Expanding the substrate scope and exploiting the mechanistic insights to increase the synthetic applicability of this catalytic method are currently being pursued in our laboratories.

EXPERIMENTAL SECTION

General Procedure for the Coupling Reaction of Phenols with Aldehydes. In a glovebox, a phenol (1.0 mmol), an aldehyde (1.0 mmol), 2-propanol (1.5 mmol), and complex **1** (3 mol %) were dissolved in 1,2-dichloroethane (1 mL) in a 25 mL Schlenk tube equipped with a Teflon stopcock and a magnetic stirring bar. The tube was brought out of the glovebox, and the contents were stirred in an oil bath preset at 120 °C for 12 h. The reaction tube was taken out of the oil bath and was cooled to room temperature. After the tube was open to air, the solution was filtered through a short silica gel column by eluting with CH_2Cl_2 (10 mL), and the filtrate was analyzed by GC-MS. Analytically pure product **2** was isolated by column chromatography on silica gel (40−63 μm particle size, hexanes/EtOAc). The product was completely characterized by NMR and GC-MS spectroscopic methods.

Computational Method. All density functional theory (DFT) calculations were performed with the Jaguar 9.1 quantum chemistry program.[31] Electronic exchange and correlation energy contributions to the total electronic energy were approximated with the B3LYP hybrid exchange functional along with Grimme's D3 dispersion correction (B3LYP-D3).[32] All intermediate and transition state geometries were optimized with the 6-31G** basis set for main-group atoms and LACVP basis set for Ru.[33,34] The LACVP basis set includes the Los Alamos relativistic effective core potentials (ECP) for Ru atoms.[34] While these basis sets are adequate for obtaining accurate geometries, more reliable energies were obtained from single-point calculations using Dunning's correlation-consistent triple-ζ basis set, cc-pVTZ(-f), for main-group atoms and LACV3P for Ru.[35] The zero-point energy (ZPE), entropic, and solvation contributions to the Gibbs energy were obtained from the same level of theory used in the geometry optimizations (B3LYP-D3/6-31G**/LACVP). The optimized geometries characterized as the local minima on the potential energy surfaces do not contain any imaginary frequencies, whereas each of the transition states contain one imaginary frequency. The solvation free energy was computed as the difference between the energy of the optimized gas-phase structure and the energy inside a solvation shell of 1,2-dichloroethane in the form of a continuum dielectric (ϵ) equaling 10.3. The electronic energy in the solvation shell was calculated using the self-consistent reaction field (SCRF) method with a Poisson−Boltzmann solver. The overall scheme for obtaining approximate solution-phase Gibbs free energies has been previously described.[36]

ASSOCIATED CONTENT

Supporting Information

The Supporting Information is available free of charge at https://pubs.acs.org/doi/10.1021/jacs.1c06887.

Experimental procedures, characterization data for organic products, and Cartesian coordinates of all computed structures and energy components (PDF)

Accession Codes

CCDC 2076966 contains the supplementary crystallographic data for this paper. These data can be obtained free of charge via www.ccdc.cam.ac.uk/data_request/cif, or by emailing data_request@ccdc.cam.ac.uk, or by contacting The Cambridge Crystallographic Data Centre, 12 Union Road, Cambridge CB2 1EZ, UK; fax: +44 1223 336033.

AUTHOR INFORMATION

Corresponding Authors

Mu-Hyun Baik − *Center for Catalytic Hydrocarbon Functionalizations, Institute for Basic Science (IBS), Daejeon 34141, Republic of Korea; Department of Chemistry, Korea Advanced Institute of Science and Technology (KAIST), Daejeon 34141, Republic of Korea;* orcid.org/0000-0002-8832-8187; Email: mbaik2805@kaist.ac.kr

Chae S. Yi − *Department of Chemistry, Marquette University, Milwaukee, Wisconsin 53233, United States;* orcid.org/0000-0002-4504-1151; Email: chae.yi@marquette.edu

Authors

Nuwan Pannilawithana − *Department of Chemistry, Marquette University, Milwaukee, Wisconsin 53233, United States*

Bimal Pudasaini − *Center for Catalytic Hydrocarbon Functionalizations, Institute for Basic Science (IBS), Daejeon 34141, Republic of Korea;* orcid.org/0000-0002-6344-7040

Complete contact information is available at: https://pubs.acs.org/10.1021/jacs.1c06887

Notes

The authors declare no competing financial interest.

ACKNOWLEDGMENTS

Financial support from the National Science of Foundation (CHE-1664652) and the National Institutes of Health General Medical Science (R15 GM109273) is gratefully acknowledged. M.-H.B. is grateful for financial support from the Institute for Basic Science (IBS-R10-A1).

REFERENCES

(1) Recent reviews: (a) Colby, D. A.; Bergman, R. G.; Ellman, J. A. Rhodium-Catalyzed C-C Bond Formation via Heteroatom-Directed C-H Bond Activation. *Chem. Rev.* **2010**, *110*, 624−655. (b) Ackermann, L. Metal-catalyzed direct alkylations of (hetero)arenes via C-H bond cleavages with unactivated alkyl halides. *Chem. Commun.* **2010**, *46*, 4866−4877. (c) Arockiam, P. B.; Bruneau, C.; Dixneuf, P. H. Ruthenium(II)-Catalyzed C-H Bond Activation and Functionalization. *Chem. Rev.* **2012**, *112*, 5879−5918. (d) Gao, K.; Yoshikai, N. Low-Valent Cobalt Catalysis: New Opportunities for C-H Functionalization. *Acc. Chem. Res.* **2014**, *47*, 1208−1219.

(2) Yamaguchi, J.; Yamaguchi, A. D.; Itami, K. C-H Bond Functionalization: Emerging Synthetic Tools for Natural Products and Pharmaceuticals. *Angew. Chem., Int. Ed.* **2012**, *51*, 8960−9009.

(3) Murai, S.; Kakiuchi, F.; Sekine, S.; Tanaka, Y.; Kamatani, A.; Sonoda, M.; Chatani, N. Efficient Ccatalytic addition of aromatic carbon-hydrogen bonds to olefins. *Nature* **1993**, *366*, 529−531.

(4) Dong, Z.; Ren, Z.; Thompson, S. J.; Xu, Y.; Dong, G. Transition-Metal-Catalyzed C-H Alkylation Using Alkenes. *Chem. Rev.* **2017**, *117*, 9333−9403.

(5) (a) Tang, R.-Y.; Li, G.; Yu, J.-Q. Conformation-induced remote *meta*-C-H activation of amines. *Nature* **2014**, *507*, 215−220. (b) Hofmann, N.; Ackermann, L. meta-Selective C-H Bond Alkylation with Secondary Alkyl Halides. *J. Am. Chem. Soc.* **2013**,

135, 5877−5884. (c) Sagadevan, A.; Greaney, M. F. *meta*-Selective C-H Activation of Arenes at Room Temperature Using Visible Light: Dual-Function Ruthenium Catalysis. *Angew. Chem., Int. Ed.* **2019**, *58*, 9826−9830.
(6) Selected examples: (a) Trost, B. M.; Imi, K.; Davies, I. W. Elaboration of Conjugated Alkenes Initiated by Insertion into a Vinylic C-H Bond. *J. Am. Chem. Soc.* **1995**, *117*, 5371−5372. (b) Colby, D. A.; Bergman, R. G.; Ellman, J. A. Stereoselective Alkylation of α,β-Unsaturated Imines via C-H Bond Activation. *J. Am. Chem. Soc.* **2006**, *128*, 5604−5605. (c) Aïssa, C.; Ho, K. Y. T.; Tetlow, D. J.; Pin-Nó, M. Diastereoselective Carbocyclization of 1,6-Heptadienes Triggered by Rhodium-Catalyzed Activation of an Olefinic C-H Bond. *Angew. Chem., Int. Ed.* **2014**, *53*, 4209−4212.
(7) (a) Xu, Y.; Dong, G. sp^3 C-H activation *via exo*-type directing groups. *Chem. Sci.* **2018**, *9*, 1424−1432. (b) Chen, Z.; Rong, M.-Y.; Nie, J.; Zhu, X.-F.; Shi, B.-F.; Ma, J.-A. Catalytic alkylation of unactivated C(sp^3)-H bonds for C(sp^3)-C(sp^3) bond formation. *Chem. Soc. Rev.* **2019**, *48*, 4921−4942.
(8) Wozniak, L.; Tan, J.-F.; Nguyen, Q.-H.; du Vigné, M. A.; Smal, V.; Cao, Y.-X.; Cramer, N. Catalytic Enantioselective Functionalizations of C-H Bonds by Chiral Iridium Complexes. *Chem. Rev.* **2020**, *120*, 10516−10543.
(9) Girard, S. A.; Knauber, T.; Li, C.-J. The Cross-Dehydrogenative Coupling of Csp^3-H Bonds: A Versatile Strategy for C-C Bond Formations. *Angew. Chem., Int. Ed.* **2014**, *53*, 74−100.
(10) (a) Chatani, N.; Asaumi, T.; Yorimitsu, S.; Ikeda, T.; Kakiuchi, F.; Murai, S. $Ru_3(CO)_{12}$-Catalyzed Coupling Reaction of sp^3 C-H Bonds Adjacent to a Nitrogen Atom in Alkylamines with Alkenes. *J. Am. Chem. Soc.* **2001**, *123*, 10935−10941. (b) Mo, F.; Dong, G. Regioselective ketone α-alkylation with simple olefins via dual activation. *Science* **2014**, *345*, 68−72. (c) Lahm, G.; Opatz, T. Unique Regioselectivity in the C(sp^3)-H α-Alkylation of Amines: The Benzoxazole Moiety as a Removable Directing Group. *Org. Lett.* **2014**, *16*, 4201−4203. (d) Lim, H. N.; Dong, G. Catalytic Intramolecular Ketone Alkylation with Olefins by Dual Activation. *Angew. Chem., Int. Ed.* **2015**, *54*, 15294−15298.
(11) He, G.; Wang, B.; Nack, W. A.; Chen, G. Syntheses and Transformations of α-Amino Acids via Palladium-Catalyzed Auxiliary-Directed sp^3 C-H Functionalization. *Acc. Chem. Res.* **2016**, *49*, 635−645.
(12) (a) Pirnot, M. T.; Rankic, D. A.; Martin, D. B. C.; MacMillan, D. W. C. Photoredox activation for the direct β-arylation of ketones and aldehydes. *Science* **2013**, *339*, 1593−1596. (b) Petronijević, F. R.; Nappi, M.; MacMillan, D. W. C. Direct β-Functionalization of Cyclic Ketones with Aryl Ketones via the Merger of Photoredox and Organocatalysis. *J. Am. Chem. Soc.* **2013**, *135*, 18323−18326.
(13) Okada, M.; Fukuyama, T.; Yamada, K.; Ryu, I.; Ravelli, D.; Fagnoni, M. Sunlight photocatalyzed regioselective β-alkylation and acylation of cyclopentanones. *Chem. Sci.* **2014**, *5*, 2893−2898.
(14) Fu, M.-C.; Shang, R.; Zhao, B.; Wang, B.; Fu, Y. Photocatalytic decarboxylative alkylations mediated by triphenylphosphine and sodium iodide. *Science* **2019**, *363*, 1429−1434.
(15) (a) Pan, S.; Shibata, T. Recent Advances in Iridium-Catalyzed Alkylation of C-H and N-H Bonds. *ACS Catal.* **2013**, *3*, 704−712. (b) Jin, J.; MacMillan, D. W. C. Alcohols as alkylating agents in heteroarene C-H functionalization. *Nature* **2015**, *525*, 87−90. (c) Su, B.; Cao, Z.-C.; Shi, Z.-J. Exploration of Earth-Abundant Transition Metals (Fe, Co, and Ni) as Catalysts in Unreactive Chemical Bond Activation. *Acc. Chem. Res.* **2015**, *48*, 886−896.
(16) (a) Lee, D.-H.; Kwon, K.-H.; Yi, C. S. Dehydrative C-H Alkylation and Alkenylation of Phenols with Alcohols: Expedient Synthesis for Substituted Phenols and Benzofurans. *J. Am. Chem. Soc.* **2012**, *134*, 7325−7328. (b) Kim, J.; Lee, D.-H.; Kalutharage, N.; Yi, C. S. Selective Catalytic Synthesis of Unsymmetrical Ethers from the Dehydrative Etherification of Two Different Alcohols. *ACS Catal.* **2014**, *4*, 3881−3885. (c) Lee, H.; Yi, C. S. Catalytic Synthesis of Substituted Indoles and Quinolines from the Dehydrative C-H Coupling of Arylamines with 1,2- and 1,3-Diols. *Organometallics* **2016**, *35*, 1973−1977.
(17) Lee, H.; Mane, M. V.; Ryu, H.; Sahu, D.; Baik, M.-H.; Yi, C. S. Experimental and Computational Study of the (*Z*)-Selective Formation of Trisubstituted Olefins and Benzo-Fused Oxacycles from the Ruthenium-Catalyzed Dehydrative C-H Coupling of Phenols with Ketones. *J. Am. Chem. Soc.* **2018**, *140*, 10289−10296.
(18) (a) Kakiuchi, F.; Murai, S. Catalytic C-H/Olefin Coupling. *Acc. Chem. Res.* **2002**, *35*, 826−834. (b) Kakiuchi, F.; Kochi, T.; Mizushima, E.; Murai, S. Room-Temperature Regioselective C-H/Olefin Coupling of Aromatic Ketones Using an Activated Ruthenium Catalyst with a Carbonyl Ligand and Structural Elucidation of Key Intermediates. *J. Am. Chem. Soc.* **2010**, *132*, 17741−17750.
(19) (a) Zdilla, M. J.; Dexheimer, J. L.; Abu-Omar, M. M. Hydrogen Atom Transfer Reactions of Imido Manganese(V) Corrole: One Reaction with Two Mechanistic Pathways. *J. Am. Chem. Soc.* **2007**, *129*, 11505−11511. (b) Neu, H. M.; Yang, T.; Baglia, R. A.; Yosca, T. H.; Green, M. T.; Quesne, M. G.; de Visser, S. P.; Goldberg, D. P. Oxygen-Atom Transfer Reactivity of Axially Ligated Mn(V)-Oxo Complexes: Evidence for Enhanced Electrophilic and Nucleophilic Pathways. *J. Am. Chem. Soc.* **2014**, *136*, 13845−13852.
(20) Kalutharage, N.; Yi, C. S. Scope and Mechanistic Analysis for Chemoselective Hydrogenolysis of Carbonyl Compounds Catalyzed by a Cationic Ruthenium-Hydride Complex with a Tunable Phenol Ligand. *J. Am. Chem. Soc.* **2015**, *137*, 11105−11114.
(21) (a) Singleton, D. A.; Thomas, A. A. High-Precision Simultaneous Determination of Multiple Small Kinetic Isotope Effects at Natural Abundance. *J. Am. Chem. Soc.* **1995**, *117*, 9357−9358. (b) Frantz, D. E.; Singleton, D. A.; Snyder, J. P. ^{13}C Kinetic Isotope Effects for the Addition of Lithium Dibutylcuprate to Cyclohexenone. Reductive Elimination Is Rate-Determining. *J. Am. Chem. Soc.* **1997**, *119*, 3383−3384. (c) Nowlan, D. T., III; Gregg, T. M.; Davies, H. M. L.; Singleton, D. A. Isotope Effects and the Nature of Selectivity in Rhodium-Catalyzed Cyclopropanations. *J. Am. Chem. Soc.* **2003**, *125*, 15902−15911. (d) Nowlan, D. T., III; Singleton, D. A. Mechanism and Origin of Enantioselectivity in the $Rh_2(OAc)$-$(DPTI)_3$-Catalyzed Cyclopropenation of Alkynes. *J. Am. Chem. Soc.* **2005**, *127*, 6190−6191.
(22) We adopted Singleton's NMR method,[21b] in which the carbon KIEs were calculated directly from the change in ^{13}C integrations from both high- and low-conversion samples of the products relative to the internal standard. Although the carbon KIE determined in this manner is somewhat less precise than the analysis obtained from using residual starting materials, the method has been shown to be sufficient for a chemical interpretation of the carbon KIEs.
(23) We previously observed that the hydride signal of triol-coordinated Ru−H complexes typically resonated at −17 to −18 ppm in ^1H NMR, which is shifted 5−7 ppm upfield from the hydride signal for **1** and other arene-coordinated Ru-H complexes: Kalutharage, N.; Yi, C. S. Chemoselective Formation of Unsymmetrically Substituted Ethers from Catalytic Reductive Coupling of Aldehydes and Ketones with Alcohols in Aqueous Solution. *Org. Lett.* **2015**, *17*, 1778−1781.
(24) Since the ^1H NMR spectra were recorded at room temperature, the complex **7** represents a "frozen" structure obtained from an early stage of the reaction. It is quite conceivable that phenol, 2-propanol, or water molecules would reversibly exchange with the coordinated aldehyde substrate at an elevated temperature, but we could not observe any definitive evidence for such a reversible coordination with different oxygen ligands during the monitored period (∼10 min).
(25) (a) Agmon, N. The Grotthuss Mechanism. *Chem. Phys. Lett.* **1995**, *244*, 456−462. (b) Polo, V.; Schrock, R. R.; Oro, L. A. A DFT Study of the Role of Water in the Rhodium-catalyzed Hydrogenation of Acetone. *Chem. Commun.* **2016**, *52*, 13881−13884.
(26) Foley, N. A.; Lee, J. P.; Ke, Z.; Gunnoe, T. B.; Cundari, T. R. Ru(II) Catalysts Supported by Hydridotris(pyarazolyl)borate for the Hydroarylation of Olefins: Reaction Scope, Mechanistic Studies, and Guides for the Development of Improved Catalysts. *Acc. Chem. Res.* **2009**, *42*, 585−597.
(27) Eitzinger, A.; Mayer, R. J.; Hampel, N.; Mayer, P.; Waser, M.; Ofial, A. R. Electrophilic Reactivities of Vinyl *p*-Quinone Methides. *Org. Lett.* **2020**, *22*, 2182−2186.

(28) (a) Bercaw, J. E.; Chen, G. S.; Labinger, J. A.; Lin, B.-L. Hydrogen Tunneling in Protonolysis of Platinum(II) and Palladium-(II) Methyl Complexes: Mechanistic Implications. *J. Am. Chem. Soc.* **2008**, *130*, 17654−17655. (b) Behnia, A.; Fard, M. A.; Blacquiere, J. M.; Puddephatt, R. J. Mild and selective Pd-Ar protonolysis and C-H activation promoted by a ligand aryloxide group. *Dalton Trans.* **2018**, *47*, 3538−3548.

(29) (a) Casey, C. P.; Johnson, J. B. Kinetic Isotope Effect Evidence for a Converted Hydrogen Transfer Mechanism in Transfer Hydrogenations Catalyzed by $[p\text{-}(Me_2CH)C_6H_4Me]Ru(NHCHPhCHPhNSO_2C_6H_4\text{-}p\text{-}CH_3)$. *J. Org. Chem.* **2003**, *68*, 1998−2001. (b) Casey, C. P.; Beetner, S. E.; Johnson, J. B. Spectroscopic Determination of Hydrogenation Rates and Intermediates during Carbonyl Hydrogenation Catalyzed by Shvo's Hydroxycyclopentadienyl Diruthenium Hydride Agrees with Kinetic Modeling Based on Independently Measured Rates of Elementary Reactions. *J. Am. Chem. Soc.* **2008**, *130*, 2285−2295.

(30) Simmons, E. M.; Hartwig, J. F. On the Interpretation of Deuterium Kinetic Isotopic Effects in C-H bond Functionalizations by Transition-Metal complexes. *Angew. Chem., Int. Ed.* **2012**, *51*, 3066−3072.

(31) Bochevarov, A. D.; Harder, E.; Hughes, T. F.; Greenwood, J. R.; Braden, D. A.; Philipp, D. M.; Rinaldo, D.; Halls, M. D.; Zhang, J.; Friesner, R. A. Jaguar: A High-Performance Quantum Chemistry Software Program with Strengths in Life and Materials Sciences. *Int. J. Quantum Chem.* **2013**, *113*, 2110−2142.

(32) (a) Becke, A. D. Density-Functional Exchange-Energy Approximation with Correct Asymptotic Behavior. *Phys. Rev. A: At., Mol., Opt. Phys.* **1988**, *38*, 3098−3100. (b) Lee, C.; Yang, W.; Parr, R. G. Development of the Colle-Salvetti Correlation-Energy Formula into a Functional of the Electron Density. *Phys. Rev. B: Condens. Matter Mater. Phys.* **1988**, *37*, 785−789. (c) Grimme, S.; Antony, J.; Ehrlich, S.; Krieg, H. A Consistent and Accurate Ab Initio Parametrization of Density Functional Dispersion Correction (DFT-D) for the 94 Elements H-Pu. *J. Chem. Phys.* **2010**, *132*, 154104.

(33) (a) Ditchfield, R.; Hehre, W. J.; Pople, J. A. Self-Consistent Molecular-Orbital Methods. IX. An Extended Gaussian-Type Basis for Molecular-Orbital Studies of Organic Molecules. *J. Chem. Phys.* **1971**, *54*, 724−728. (b) Hehre, W. J.; Lathan, W. A. Self-Consistent Molecular Orbital Methods. XIV. An Extended Gaussian-Type Basis for Molecular Orbital Studies of Organic Molecules. Inclusion of Second Row Elements. *J. Chem. Phys.* **1972**, *56*, 5255−5257. (c) Rassolov, V. A.; Ratner, M. A.; Pople, J. A.; Redfern, P. C.; Curtiss, L. A. 6-31G* Basis Set for Third-Row Atoms. *J. Comput. Chem.* **2001**, *22*, 976−984.

(34) (a) Hay, P. J.; Wadt, W. R. Ab Initio Effective Core Potentials for Molecular Calculations. Potentials for the Transition Metal Atoms Sc to Hg. *J. Chem. Phys.* **1985**, *82*, 270−283. (b) Wadt, W. R.; Hay, P. J. Ab Initio Effective Core Potentials for Molecular Calculations. Potentials for Main Group Elements Na to Bi. *J. Chem. Phys.* **1985**, *82*, 284−298. (c) Hay, P. J.; Wadt, W. R. Ab Initio Effective Core Potentials for Molecular Calculations. Potentials for K to Au Including the Outermost Core Orbitals. *J. Chem. Phys.* **1985**, *82*, 299−310.

(35) (a) Dunning, T. H. Gaussian Basis Sets for Use in Correlated Molecular Calculations. I. The Atoms Boron through Neon and Hydrogen. *J. Chem. Phys.* **1989**, *90*, 1007−1023. (b) *LACV3P: a triple-zeta contraction of the LACVP basis set*; Schrodinger Inc.

(36) Ryu, H.; Park, J.; Kim, H. K.; Park, J. Y.; Kim, S.-T.; Baik, M.-H. Pitfalls in Computational Modeling of Chemical Reactions and How to Avoid them. *Organometallics* **2018**, *37*, 3228−3239.

https://doi.org/10.1021/jacs.1c06887
J. Am. Chem. Soc. 2021, 143, 13428−13440